Int'l Journal of Advances in Chemical Engg., & Biological Sciences (IJACEBS) Vol. 4, Issue 1 (2017) ISSN 2349-1507 EISSN 2349-1515

Characterization and spectroscopic study of a heat-treated and acid-leached halloysite used in Congo red adsorption

Fatiha Bessaha, Souhila Bendenia, Nouria Mahrez, Fatima Kasmi, Kheira Marouf, Amine Khelifa

Abstract— Algerian halloysite was heated at 600 °C and treated with HCl 5N. The materials were characterized by chemical analysis, TEM, and FT-IR spectroscopy, and used in the elimination of Congo red (CR) from aqueous solution. The effects of contact time and temperature were investigated. The thermal treatment at 600 °C results in the formation of dehydroxylated structure. Acid attack involves an increase in SiO_2 content, due to the leaching of Al ions from octahedral sheet. Thermo-chemical treatment also diminishes the percentage of impurities and maintains the tubular morphology. Kinetic data follow the pseudo-second order model, whilst thermodynamic parameters lead to a not spontaneous and endothermic process. Significant changes occur in the vibrational spectrum of H600-5N (halloysite treated at 600 °C and with HCl 5N), after adsorption of Congo red, with the involvement of amino and sulfoxide groups. The mechanism highlights an outer-sphere surface complexation of SiOH....H_2O species, i.e., SiOH linked to H_2O via H-bonds.

Keywords— Halloysite, Characterization, Adsorption, FTIR.

I. INTRODUCTION

Azo dyes are an important class of dyes that are widely used in the textile, leather, rubber, paper, and cosmetic industries [1]. After use, azo dyes are generally released into effluents. Their presence in wastewaters causes serious problems for the environment and living organisms, because they are highly resistant to degradation, carcinogenic due to the presence of aryl amines, and persistent in the environment for an extended period of time [2]. A variety of techniques are available nowadays for treating these contaminants. Among these may be mentioned advanced oxidation [3], ozonation [4], biological treatment [5], membrane separation [6], and precipitation [7]. Advanced oxidation processes are considered to be high-cost methods. Biodegradation suffers from optimization problems in addition to the relatively biorefractory character of these dyes. The membrane processes require their frequent change, while precipitation produces a large amount of sludge and is not suitable for removing low concentrations. Adsorption is especially attractive because of its high efficiency, simplicity of design, and ease of operation [8].

Different adsorbents were used to adsorb Congo red (CR), an azo dye, from aqueous solutions, such as activated carbon [9], chitosan [10], carbon nanotubes [11], cashew nut shell [12] fly ash [13], rice hull ash [14], and leaf [15]. However, their methods of modification and/or their costly regeneration limit their application. Clays are low cost materials, eco-friendly, and abundant in the nature.

The aim of the study is to examine the ability of modified halloysites for removing RC from synthetic solutions. Three halloysitic solids were used, viz. unmodified halloysite (H), the form calcined at 600 °C (H600), and that processed at 600 °C and with 5N HCl (H600-5N). After characterization, the adsorption of RC was studied by taking into account the effects of kinetics and temperature. A particular interest has been focused on the FTIR study, before and after adsorption. The objective is to understand the uptake mechanism of Congo red.

II. MATERIALS AND METHODS

2.1. Materials

Halloysite used in this work is from Djebel Debbagh (Algeria). Its characteristics were reported in a previous work [16]. A certain amount of the starting material was heated at 600 ˚C for 2 h in air atmosphere. Thereafter, 45 g of H600 was mixed with 1125 mL of HCl solution 5N. The suspension was stirred at 70 ˚C for 4 h then filtered. The recovered solid was abundantly washed with distilled water and dried at 110 ˚C for 2 h.

2.2. Characterization

Chemical analysis and the SiO_2/Al_2O_3 molar ratio of the halloysitic solids were determined by ICP-AES on a Perkin-Elmer instrument. TEM images were performed on a JEOL 2100 electron microscope. An EDX detector for X-ray energy dispersive analysis was attached to this microscope. Infrared spectra were recorded with a Shimadzu 1240 FT-IR spectrometer (resolution 2 cm^{-1}). The 4,000–400 cm^{-1} region was studied.

2.3. *Adsorption* procedure

A stock solution of Congo red (CAS No: 573-58-0, chemical formula : $C_{32}H_{22}N_6Na_2O_6S_2$, FW: 696.67 g mol^{-1}, λ_{max}= 498 nm, supplier : Biochem Chemopharma) of concentration 80 mg L^{-1} was prepared. The experiments were performed via the batch method.

Fatiha Bessaha[1] Laboratoire de Structure, Elaboration et Applications des Mate´riaux Mole´culaires (S.E.A.2M.), De´partement de Chimie, Universite´
de Mostaganem, B.P. 981, R.P., Mostaganem 27000, Algeria; (corresponding author's phone: Tel. +213 45 21 60 80; e-mail: fatiha_bessaha@yahoo.fr).
Fatima Kasmi[4], Laboratoire de Structure, Elaboration et Applications des Mate´riaux Mole´culaires (S.E.A.2M.), De´partement de Chimie, Universite´
de Mostaganem, B.P. 981, R.P., Mostaganem 27000, Algeria; (e-mail: fatima21.kasmi@hotmail.fr).

https://doi.org/10.15242/IJACEBS.C0417032

0.02 g of halloysitic solid was mixed with 20 mL of aqueous CR solution. pH of the dispersions was adjusted to 6. After each experiment, the solution was separated by centrifugation, then the supernatant was analyzed by visible spectrophotometry at 498 nm, using a Shimadzu 1240 UV–Vis spectrophotometer. The adsorbed amount was calculated from the difference between the initial and final concentrations. The effects of contact time and temperature were studied.

2.4. Theoretical considerations

In order to investigate the mechanism controlling adsorption, different equations were applied to model the kinetics of Congo red adsorption onto our materials.

Lagergren [17] proposed a pseudo-first order kinetic model. Its integral form is

$$\log(Q_e - Q_t) = \log Q_e - \frac{K_1 t}{2.303} \qquad (1)$$

where Q_t is the amount adsorbed at time t (mg/g), Q_e, the adsorption capacity at equilibrium (mg/g), K_1, the pseudo-first order rate constant (min^{-1}), and t is the contact time (min).

Kinetics may also be described by a pseudo-second order reaction. Its linearized-integral form is [18]:

$$\frac{t}{Q_t} = \frac{1}{K_2 Q_e^2} + \frac{t}{Q_e} \qquad (2)$$

where K_2 (g mg^{-1} min^{-1}) is the pseudo-second order rate constant. The initial rate, h, as t→0 can be defined as

$$h = K_2 . Q_e^2 \qquad (3)$$

The plot of t/Q_t vs. t should give a linear relationship, from which K_2 and h can be determined from the slope and the intercept of the plot.

During adsorption under batch mode, there is a possibility of transport of adsorbate species into the pores of adsorbent, which is often the rate controlling step. The intraparticle diffusion rate equation can be written as follows [19]:

$$Q_t = K_{id} t^{1/2} + C \qquad (4)$$

where K_{id} (mg g^{-1} $min^{-1/2}$) is the intraparticle diffusion rate constant and C, a constant. The K_{id} and C values are calculated from the slope and the intercept of the plot of Q_t versus $t^{1/2}$, respectively.

2.4.2. Thermodynamic study

The parameters ΔH^0, ΔS^0, and ΔG^0 were evaluated using the following equation

$$\ln K_d = (-\Delta H^0/R.T) + (\Delta S^0/R) \qquad (5)$$

where ΔH^0 (kJ $mole^{-1}$) and ΔS^0 (J $mole^{-1}$ K^{-1}) are enthalpy and entropy changes, respectively; T (K), absolute temperature; R (J mol^{-1} K^{-1}), gas constant; K_d (L g^{-1}), distribution coefficient, which is given by

$$K_d = Q_e / C_e \qquad (6)$$

Enthalpy and entropy changes are graphically determined by plotting ln K_d versus 1/T, which gives a straight line. According to thermodynamics, the Gibbs free energy change, ΔG^0, is related to ΔH^0 and ΔS^0 by the following equation

$$\Delta G^0 = \Delta H^0 - T\Delta S^0 \qquad (7)$$

III. RESULTS AND DISCUSSION

3.1. Characterization

3.1.1. Chemical Analysis

Chemical compositions of the halloysitic solids are presented in Table 1. Raw halloysite (H) contains alumina and silica in major quantities, contrary to other oxides. When halloysite is treated at 600 °C (H600), its SiO_2/Al_2O_3 molar ratio increases slightly from 1.81 to 1.92, consequence of the dehydroxylation of structural aluminol groups [20]. After thermochemical modification, the chemical composition of H600-5N changes profoundly. Molar ratio increases up to 27.11, while the percentage of Fe_2O_3, CaO, MgO, and MnO diminishes considerably. The decrease in alumina content can be ascribed to the leaching of the Al^{3+} ions from the octahedral sheet [21]. Acid attack also leads to the elimination of a great part of impurities [22].

Table 1. Chemical composition of raw and modified halloysite

Samples	SiO_2 (%)	Al_2O_3 (%)	CaO (%)	Fe_2O_3 (%)	K_2O (%)	MgO (%)	MnO (%)	Na_2O (%)	Molar ratio SiO_2/Al_2O_3
H	49.1	46.16	0.94	1.25	0.31	0.21	1.44	0.54	1.81
H600-0N	44.7	39.69	0.65	0.45	0.32	0.05	2.01	0.34	1.92
H600-5N	73.0	4.59	0.03	0.09	0.30	0.003	0.05	0.16	27.11

3.1.2. Transmission electron microscopy

TEM images of H600 and H600-5N are presented in Fig.1. H600 highlights particles having a cylindrical shape and containing a transparent central area that runs longitudinally along the cylinder. The nanotubular particles obtained are hollow and open-ended. Their size is different both in diameter and length. Their external and internal diameters vary from 30 to 180 nm and from 10 to 30 nm, respectively. These rolled tubes consist in a number of aluminosilicate layers curved and closely packed. This morphology was also obtained for the unmodified halloysite [23], proving that the thermal treatment at 600 °C conserves the tubular nature of the Algerian halloysite. A phase rich in Mn, Al, and O was evidenced by EDX in microscope. This phase consists in agglomerated small plates of diameter 10 nm. Interlayer spacing could not be highlighted. This is probably due to the fact that the layers are immediately destroyed under the beam of electrons.

The sample H600-5N (Fig.1) also leads to a tubular morphology, although the tubes obtained are somewhat damaged. Dehydroxylation associated with the leaching of Al^{3+} alter slightly the nanotubes. The observation of the morphological details is of a great relevance. The defects on the surface such as surface breakage or crystallographic defects could prove as potential reaction sites for the surface chemistry of halloysitic clays.

3.2. Congo red adsorption

3.2.1. Kinetics

The effect of contact time is reported in Fig. 2. Adsorption rate is rapid in the first 10 min, then it decreases continuously, reaching equilibrium at about 2 h. So, an agitation time of 2 h seems to be sufficient for equilibrium experiments. Fast initial adsorption could be attributed to the presence of a great number of vacant sites and a high gradient of solute concentrations [24]. Highest capacity in CR adsorption was found for H600-5N.

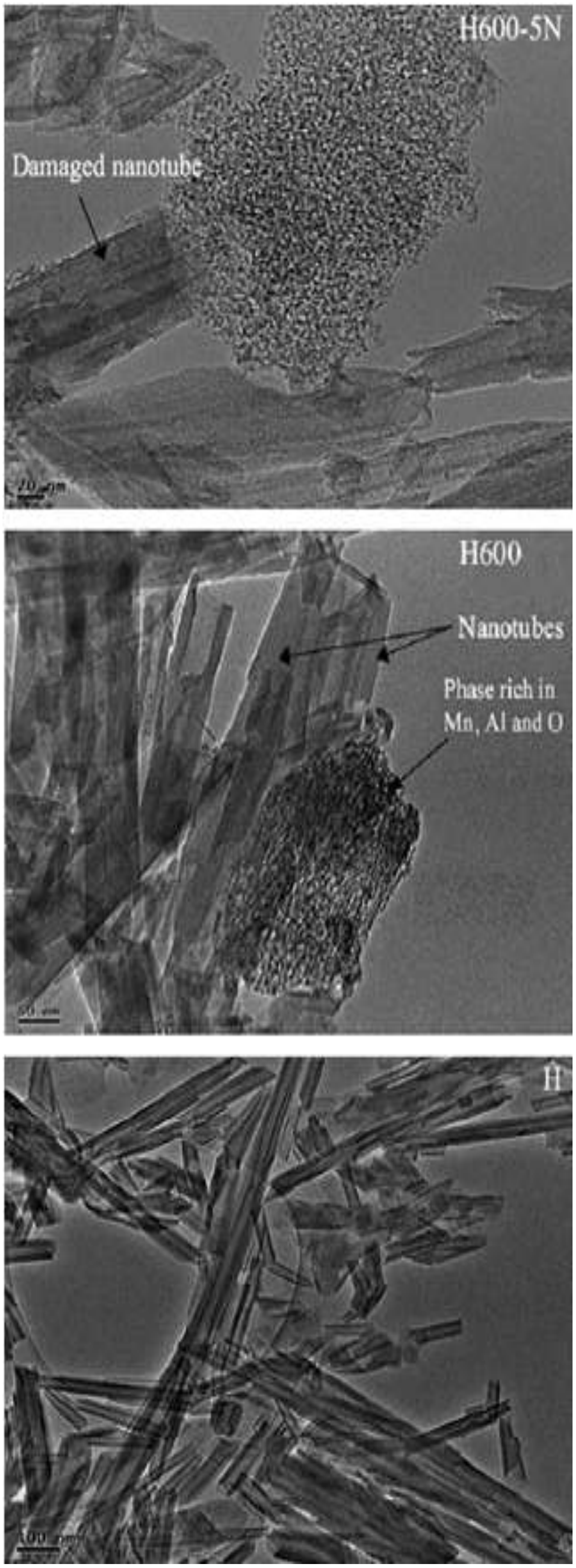

Fig 1.Transmission electron microscopy images of H, H600, and H600-5N.

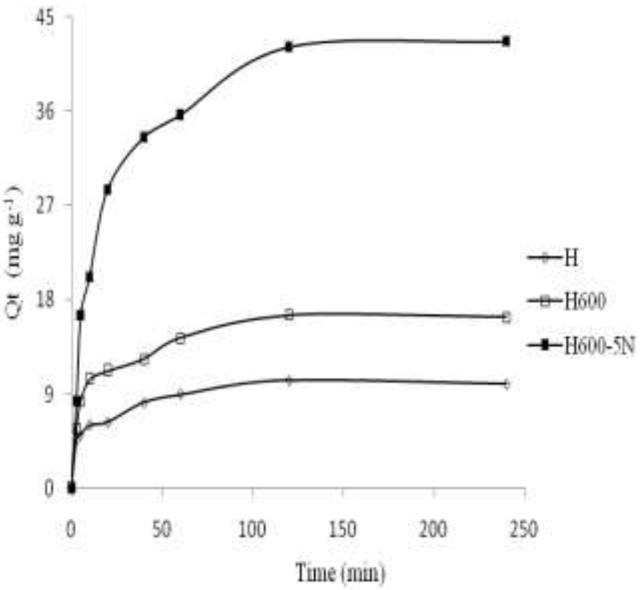

Fig. 2. Effect of contact time on the uptake CR of H, H600 and H600-5N, at 55 °C.

The parameters of the kinetic models used are presented in Table 2. The pseudo-first order equation does not apply, because the estimated theoretical quantities, Q_e (cal), are different from the experimental values, Q_e (exp). Also, the curves diverge from linearity (Fig. 3). The fit of the experimental data with the pseudo-second order model is more suitable.

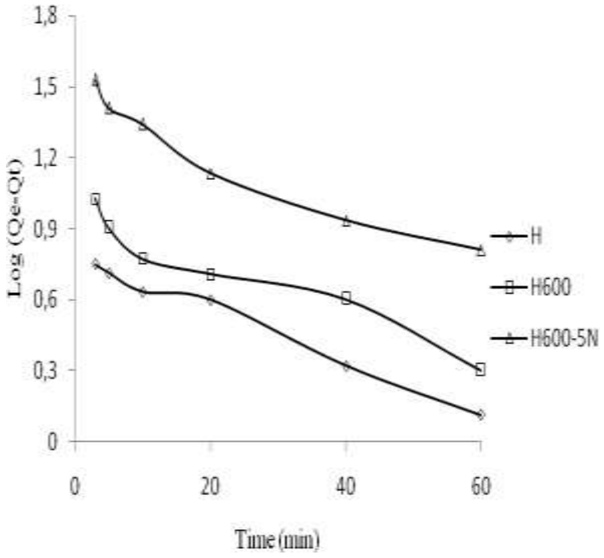

Fig. 3.Pseudo first order kinetic for the adsorption of CR onto halloysitic solids

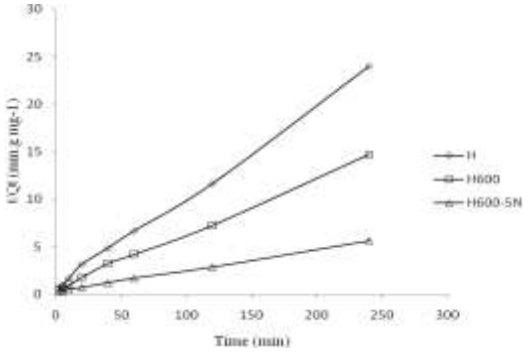

Fig 4. Pseudo second order kinetic for the adsorption of CR onto halloysitic solids

Linear plots of t/Qt vs. t (Eq. 2) were obtained (Fig. 4), corresponding to high R^2 values, i.e., ≥ 0.99, while the Q_e (cal) values are closely linked to those of Q_e (exp). The use of the intraparticle diffusion model requires the plotting Qt against $t^{1/2}$ (Fig. 5). This model is not the only rate-controlling step, due to the deviation of the plots from the origin (C values ≠ 0, Table 2). As consequence, the boundary layer diffusion affects the CR adsorption to some extents. The values of intercept, C, give an idea about the thickness of boundary layer, i.e., the larger the intercept, the greater is the boundary layer effect [25]. The C values of H600-5N rise considerably compared to those of the unmodified halloysite. At 55 °C, it is 3.32 times larger than that of H. Treatment with HCl disrupts the interfacial properties of halloysitic clay, so the effect of boundary layer plays a prominent role.

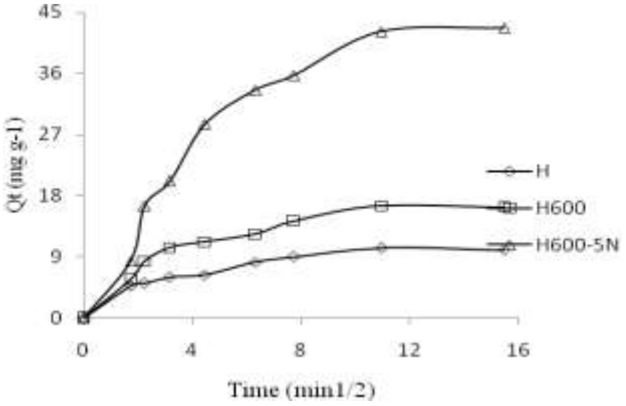

Fig 5. Intraparticle diffusion effect on the adsorption of CR ion onto halloysitic solids

3.2.2. Thermodynamics

The values of free energy (ΔG°), enthalpy (ΔH°), and entropy (ΔS°) are listed in Table 3. The ΔG° values are positive in the temperature range studied, revealing a process not spontaneous with possibility of chemisorption [26]. These values decrease with increasing temperature regardless of the material, indicating that better adsorption is obtained at higher temperatures. The positive ΔH° values highlight the endothermic character of CR adsorption. The process is, thus, favored by an increase in temperature via the activation of the adsorption sites [27]. The positive entropies suggest an increase in randomness at the solid–solution interface, for which significant changes occur in the internal structure of the adsorbents, after adsorption. [28].

TABLE II: KINETIC PARAMETERS FOR CR ADSORPTION ONTO MODIFIED HALLOYSITES

			Pseudo-first-order model			Pseudo-second order model				Intraparticle diffusion model		
Samples	**T(°C)**	**Q_t(exp) (mg g^{-1})**	**Q_t(cal) (mg g^{-1})**	**K_1 (min^{-1})**	**R^2**	**Q_t(cal) (mg g^{-1})**	***K_2* (g $mg^{-1}min^{-1}$)**	***h* (mg $g^{1}min^{-1}$)**	**R^2**	***K_{id}* (mg $g^{-1}min^{-1/2}$)**	***C* (mg g^{-1})**	**R^2**
H	25	21.05	16.71	0.037	0.991	22.22	0.0042	2.09	0.999	2.54	0.97	0.979
	40	28.32	23.60	0.025	0.975	32.26	0.0016	1.69	0.998	3.22	1.06	0.999
	55	10.30	5.96	0.025	0.989	10.42	0.0013	1.41	0.997	0.72	3.52	0.952
H600	25	32.28	26.92	0.035	0.984	34.48	0.0021	2.48	0.998	3.11	5.46	0.969
	40	25.65	18.45	0.035	0.976	27.07	0.0039	2.87	0.998	2.04	7.11	0.985
	55	16.54	9.27	0.023	0.926	16.95	0.0072	2.07	0.997	0.83	7.58	0.955
H600-5N	25	25.43	16.48	0.014	0.781	27.78	0.0022	1.68	0.990	0.90	9.95	0.999
	40	38.02	28.12	0.021	0.977	41.67	0.0015	2.60	0.995	2.80	10.16	0.996
	55	42.12	29.51	0.028	0.937	45.45	0.0018	3.76	0.999	3.27	11.70	0.919

TABLE III: THERMODYNAMIC PARAMETERS FOR THE CR ADSORPTION ONTO MODIFIED HALLOYSITES

Samples	**ΔH (kJ $mole^{-1}$)**	**ΔS (kJ mole. K^{-1})**	**ΔG (kJ $mole^{-1}$)**		
			25 °C	**40 °C**	**55 °C**
H	8.31	0.010	5.22	5.07	4.91
H600	12.69	0.025	5.22	4.85	4.47
H600-5N	12.67	0.028	4.44	4.03	3.61

3.2.3. FTIR analysis

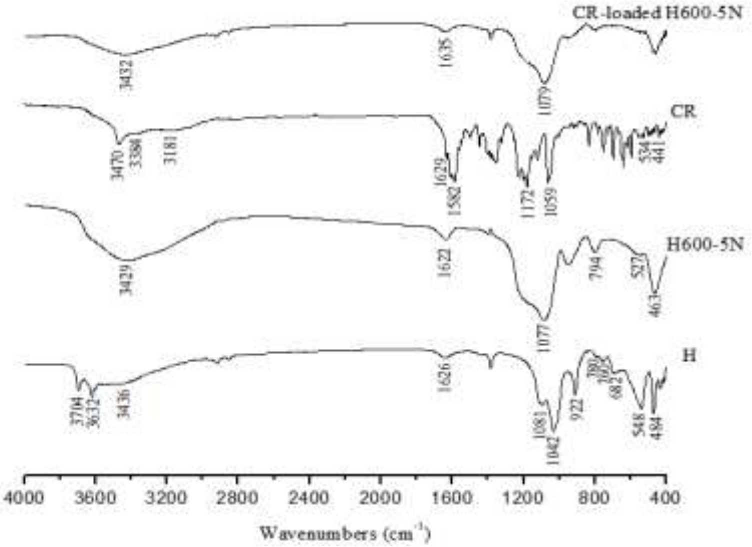

Fig 6. FTIR spectra of H, H600-5N, CR, and CR-loaded H600-5N

https://doi.org/10.15242/IJACEBS.C0417032

The infrared spectra of H, H600-5N, CR, and CR-loaded H600-5N (H600-5N after adsorption of Congo red), were recorded in the 4000–400 cm^{-1} range and depicted in (Fig. 6).

The FTIR spectrum of the starting material (Fig. 6–H) shows two bands at 3704 and 3632 cm^{-1} attributed to the stretching vibrations of the inner surface and inner sheet hydroxyls, respectively [29]. The band at 3436 cm^{-1} indicates the stretch of interlayer water. The 1626 cm^{-1} band represents the hydration of δAlOH [30]. The 1081 cm^{-1} band is assigned to the stretching mode of apical Si–O, whilst those at 1042 and 922 cm^{-1} are caused by the stretch of Si–O–Si and the bending of Al–O–H, respectively [31]. The bands at 548 and 484 cm^{-1} are attributed to Al–O–Si and Si-O-Si bendings, respectively.

Significant changes occur in the vibrational spectrum when halloysite was heat-treated and acid-leached (Fig. 6–H600-5N). The broadening of the 3429 cm^{-1} band reveals the formation of silica nanoparticles [32]. The persistence of 1622 cm^{-1} band may be assigned to the hydration of δSiOH instead of AlOH, given the elimination of Al by acid attack. The abatement of the stretch at 1081 cm^{-1}, the widening of the 1077 cm^{-1} band, the disappearance of the vibrations at 760 (Si–O–Al perpendicular stretching) and 682 cm^{-1} (Si–O–Al), the decrease in the band at 527 cm^{-1}, show the formation of amorphous silica [33] and the elimination of aluminium from octahedral sheets [32]. This interpretation is in conformity with the evolution of SiO_2/Al_2O_3 molar ratio, which increases from 2.08 (H) to 27.11 (H600-5N) (Table 1).

The spectrum of Congo red before adsorption (Fig. 6–CR) exhibits bands at 3470 and 3384 cm^{-1} due to the asymmetrical and symmetrical N-H stretches of primary amines, respectively [34]. The 3181 cm^{-1} band is associated with C-H vibrations in aromatic rings. The N-H bending of primary amine occurs at 1630 cm^{-1}. The band at 1451 cm^{-1} is indicative of the vibration of C=C bonds in the aromatic ring. The asymmetric and symmetric vibrations of S=O in sulfonate groups appear at 1172 and 1059 cm^{-1}, respectively. Medium bands arise in the 900-650 cm^{-1} range, indicating N-H wagging, while that at 534 cm^{-1} is due to torsional N-H oscillation.

The results of H600-5N after exposure to a solution of 400 mg L^{-1} of CR (Fig. 6–CR-loaded H600-5N) highlight some modifications of the absorption bands: some vanish while others are found to shift. The 3432 and 1631 cm^{-1} bands decrease in intensity and shift slightly after CR adsorption, denoting a deep involvement of amino groups [34]. The same behavior was obtained for the bands at 1172 and 1059 cm^{-1} (asymmetric and symmetric vibrations of S=O), which indicates the implication of sulfonate anions via S=O groups. The shift of 1622 band towards 1635 cm^{-1} and the decrease of its intensity prove that RC molecules interact with $SiOH(H_2O)$ species.

Goyne et al. [35] showed that the proton dissociation on silanol surface sites starts at circumneutral pH. Bearing in mind that adsorption was performed at pH 6, the interaction of AH600-5N occurs via SiOH groups. The latter are bound to H_2O via H-bonds, forming SiOH....H_2O species [36]. On the basis of the spectroscopic study, the mechanism is an outer-sphere surface complexation of SiOH....H_2O (H600-5N) by Congo red molecules via amine (NH_2) and sulfoxide (S=O) groups, which provide the nonbonding electrons from nitrogen and sulfur atoms, respectively.

IV. CONCLUSION

Thermo-chemical modification of halloysite at 600 °C and with HCl 5N leads to dehydroxylation of the structure and the leaching of Al ions from octahedral sheet. As consequence, SiO_2/Al_2O_3 molar ratio increases from 1.81 to 27.11. This treatment maintains the tubular nature of our halloysite. The kinetics of Congo red adsorption follows the second-pseudo order model with a contribution of intraparticle diffusion. Thermodynamic parameters highlight a not spontaneous and endothermic character. Spectroscopic study shows an outer-sphere surface complexation between SiOH....H_2O and nonbonding electrons of nitrogen and sulfur atoms of amine (NH_2) and sulfoxide (S=O) groups, respectively.

REFERENCES

[1] S. Dawood, T. K. Sen, Removal of anionic dye Congo red from aqueous solution by raw pine and acid-treated pine cone powder as adsorbent, equilibrium, thermodynamic, kinetics, mechanism and process design. Water, Res. 2012. 46. 1933–1946.

[2] A. R, Gregory, S. Elliot, P. Kluge, Ames testing of direct black 3B parallel carcinogenicity. Journal of Applied Toxicology 1991. 13. 1-308.

[3] W. Chen, Lu, Wangyang, Y. Yao, M. Xu, Highly efficient decomposition of organic dyes by aqueous-fiber phase transfer and in situ catalytic oxidation using fiber-supported cobalt phthalocyanine. Environ. Sci. Technol. 2007. 41. 6240–6245.

[4] X. Zhang, W. Dong, F. Sun, W. Yang, J. Dong, Degradation efficiency and mechanism of azo dye RR2 by a novel ozone aerated internal microelectrolysis filter, J. Hazard. Mater. 2014. 276. 77–87.

[5] D. Cui, Y. Q. Guo, H. S. Lee, H. Y. Cheng, B. Liang, F. Y. Kong, Y. Z. Wang, L. P. Huang, M. Y. Xu, A. J. Wang, Efficient azo dye removal in bioelectrochemical system and post-aerobic bioreactor: optimization and characterization, Chem. Eng. J. 2014. 243 355–363.

[6] S. Cheng, D. L. Oatley, P. M. Williams, C. J. Wright, Characterisation and application of a novel positively charged nanofiltration membrane for the treatment of textile industry wastewaters. Water Res. 2012. 46, 33–42.

[7] B. Ismail, S. T. Hussain and S. Akram, Chem. Eng. J. 2013. 219. 395–402.

[8] A. Gurses C. Dogar M. Yalcin M. Acikyildiz R. Bayrak S. Karaca, The adsorption kinetics of the cationic dye, methylene blue, onto clay. Journal of Hazardous Materials 2006. 131.

[9] S. Chatterjee, D. S. Lee, Min W. Lee, S. H. Woo, Enhanced adsorption of congo red from aqueous solutions by chitosan hydrogel beads impregnated with cetyl trimethyl ammonium bromide, Bioresource Technology 2009. 100 2803–2809,

[10] T. Panczyk, P. Wolski, A. Jagusiak, M. Drach, Molecular dynamics study of Congo red interaction, with carbon nanotubes, RSC Adv., 2014. 4, 47304.

[11] F. A. Pavan, S. L.P. Dias, E. C. Lima, E. V. Benvenutti, Removal of Congo red from aqueous solution by anilinepropylsilica xerogel, Dyes and Pigments 2008. 76 64- 69

[12] P. Senthil Kumar, S. Ramalingam, C. Senthamarai, M. Niranjanaa, P. Vijayalakshmi, S. Sivanesan, Adsorption of dye from aqueous solution by cashew nut shell: Studies on equilibrium isotherm, kinetics and thermodynamics of interactions Desalination 2010. 261. 52–60

[13] I. D. Mall, V. C. Srivastava, N. K. Agarwal, I. M. Mishra, Removal of congo red from aqueous solution by bagasse fly ash and activated carbon: kinetic study and equilibrium isotherm analyses. Chemosphere 2005. 61. 492–501.

[14] K. S. Chou, J. C. Tsai, C. T. Lo, The adsorption of congo red and vacuum pump oil by rice hull ash. Bioresour. Technol. 2001. 78. 217–219.

[15] K. G. Bhattacharrya, A. Sharma, Azadirachta indica leaf powder as an effective biosorbent for dyes: a case study with aqueous congo red solutions. J. Environ. Manage. 2004. 71 217–229.

[16] S. Mellouk, S. Cherifi, M. Sassi, K. Marouf-Khelifa, A. Bengueddach, J. Schott, A. Khelifa, Intercalation of halloysite from Djebel Debagh (Algeria) and adsorption of copper ions,Appl. Clay Sci. 2009. 44 230–236.

[17] S. Lagergren, Zur theorie der sogenannten adsorption geloster stoffe (About the theory of so-called adsorption of soluble substances), Kungliga SvenskaVetenskapsademiens, Handlingar (K. Sven. Vetenskapsakad. Handl.) 1898. 24. 1–39.

[18] Y.S. Ho, G. McKay, Pseudo-second order model for sorption processes, Process Biochem. 1999. 34 451–465.

[19] W. J. Weber, J. C. Morris, Kinetics of adsorption on carbon from solution, J. Sanitary Eng. Div. Am. Soc. Civ. Eng. 1963. 89. 31–59.

[20] P. Yuan, P. D. Southon, Z. Liu, M. E. R. Green, J. M. Hook, S. J. Antill, C. J. Kepert, Phys. Chem. C 2008.112 15742–15751.

[21] A. K. Panda, B. G. Mishra , D. K. Mishra , R. K. Singh, Effect of sulphuric acid treatment on the physico-chemical characteristics of kaolin clay, Colloids and Surfaces A: 363 (2010) 98–104.

[22] J.D.D. Melo, T.C.C. Costa, A.M. Medeiros, C.A. Paskocimas, Effects of thermal and chemical treatments on physical properties of kaolinite, Ceramics International 2010. 36 33–38

[23] S. Mellouk, A. Belhakem, K. Marouf-Khelifa, J. Schott, A. Khelifa, Cu(II) Adsorption By halloysites intercalated with sodium acetate, J. Colloid Interface Sci. 201. 360. 716–724.

[24] L. Zhang, H. Zhang, W. Guo, Y. Tian, Removal of malachite green and crystal violet cationic dyes from aqueous solution using activated sintering process red mud, Applied Clay Science 93. 2014. 85–93.

[25] N. K. Kannan, M. M. Sundaram, Kinetics and mechanism of removal of methylene blue by adsorption on various carbons-A comparative study, Dyes Pigm. 2001 51. 25–40.

[26] Y. Salameh, N. Al-Lagtah, M.N.M. Ahmad, S.J. Allen, G.M. Walker, Kinetic and thermodynamic investigations on arsenic adsorption onto dolomitic sorbents, Chem. Eng.J. 2010. 160. 440-446

[27] K. Vijayaraghavan, Yeoung-Sang Yun, Biosorption of C.I. Reactive Black 5 from aqueous solution using acid-treated biomass of brown seaweed Laminaria sp., Dyes and Pigments 76 (2008) 726−732.

[28] M. Alkan, O. Demirbas¸, M. Dogan, Adsorption kinetics and thermodynamics of an anionic dye onto sepiolite, Microporous Mesoporous Mater. 2007. 101. 388–396.

[29] N. Mahrez, S. Bendenia, K. Marouf-Khelifa, I. Batonneau-Gener, A. Khelifa, Improving of the adsorption capacity of halloysite nanotubes intercalated with dimethyl sulfoxide, J Composite Interfaces 22 (2015) 403-417.

[30] E. Srasra, F. Bergaya, J.J. Fripiat, Infrared spectroscopy study of tetrahedral and octahedral substitutions in an interstratified illite-smectite, clay clays and clay minerals. 42 (1994) 237–241.

[31] Y. Deng, G.N. White, J.B. Dixon, Effect of structural stress on the intercalation rate of kaolinite, J. Colloid Interface Sci.250 (2002) 379–393.

[32] E. Abdullayev, A. Joshi, W. Wei, Y. Zhao, Y. Lvov, Enlargement of halloysite clay nanotube lumen by selective etching of aluminum oxide. ACS Nano 6 (2012) 7216–7226.

[33] J.P. Nguetnkam, R. Kamga, F. Villie ´ras, G.E. Ekodeck, A. Razafitianamaharavo, J. Yvon, Assessment of the surface areas of silica and clay in acid- leached clay materials using concepts of adsorption on heterogeneous surfaces, J. Colloid Interface Sci. 289 (2005) 104–115.

[34] R.M. Silverstein, G.C. Bassler, T.C. Morrill, Spectrometric Identification of the Organic Compounds, fifth ed., De Boeck Universite´, Bruxelles, 1998. (in French).

[35] K.W. Goyne, Surface Charge of Variable Porosity Al_2O_3(s) and SiO_2(s) Adsorbents, J. Porous Mater 9. (2002) 243–256.

[36] L.T. Zhuravlev, The surface chemistry of amorphous silica. Zhuravlev model, Colloids and Surf A. 173 (2000) 1–38.

https://doi.org/10.15242/IJACEBS.C0417032